HOCCO versus OCCO: Comparative spectroscopy of the radical and diradical reactive intermediates

Andrew R. Dixon, Tian Xue, and Andrei Sanov[a)]
Department of Chemistry and Biochemistry, The University of Arizona, Tucson, Arizona 85721, USA

(Received 15 April 2016; accepted 31 May 2016; published online 15 June 2016)

We present a photoelectron imaging study of three glyoxal derivatives: the ethylenedione anion ($OCCO^-$), ethynediolide ($HOCCO^-$), and glyoxalide ($OHCCO^-$). These anions provide access to the corresponding neutral reactive intermediates: the OCCO diradical and the HOCCO and OHCCO radicals. Contrasting the straightforward deprotonation pathway in the reaction of O^- with glyoxal (OHCCHO), which is expected to yield glyoxalide ($OHCCO^-$), $OHCCO^-$ is shown to be a minor product, with $HOCCO^-$ being the dominant observed isomer of the $m/z = 57$ anion. In the HOCCO/OHCCO anion photoelectron spectrum, we identify several electronic states of this radical system and determine the adiabatic electron affinity of HOCCO as 1.763(6) eV. This result is compared to the corresponding 1.936(8) eV value for ethylenedione (OCCO), reported in our recent study of this transient diradical [A. R. Dixon, T. Xue, and A. Sanov, Angew. Chem., Int. Ed. **54**, 8764–8767 (2015)]. Based on the comparison of the $HOCCO^-$/$OHCCO^-$ and $OCCO^-$ photoelectron spectra, we discuss the contrasting effects of the hydrogen connected to the carbon framework or the terminal oxygen in OCCO. *Published by AIP Publishing.* [http://dx.doi.org/10.1063/1.4953774]

I. INTRODUCTION

Anion photodetachment provides access to the ground and excited states of neutral molecules without regard for their transient or stable nature. Moreover, states of different multiplicities can be probed at the same time, provided the photon energy used is sufficient and there is sizable Franck-Condon (FC) overlap between the anion equilibrium and the neutral states of interest.

This feature of anion photoelectron spectroscopy has been used to study a variety of exotic neutral species, including transient molecules, reactive intermediates, and even transition states, all of which are challenging to access using other methods.[1–5] Here, we present a comparative analysis of three glyoxal derivatives, the OHCCO and HOCCO radicals and the OCCO diradical, all three of which are generated via the photodetachment of the corresponding anions. The spectroscopy of HOCCO is reported for the first time, while the discussion of OCCO builds upon our recent brief report[6] of the discovery of this molecule.

The spectroscopic characterization of the ethylenedione molecule, OCCO, was accomplished recently[6] against the backdrop of a century-long history of failed attempts to detect this species. Despite its apparent yet deceptive simplicity, reflected in the straightforward Kekulé structure O=C=C=O, ethylenedione is a short-lived reactive intermediate.[7,8] Its existence was first proposed in 1913,[9] but all previous experimental strategies tried ever since had failed to produce conclusive evidence that OCCO really existed.[7,8,10–14] The molecule was at long last found in 2015,[6] via the photodetachment of its stable[15,16] anion. The results shed light on the manifold of low-lying electronic states of OCCO,[6] confirming the past predictions of its electronic structure.

In short, the ground quasi-bound state of OCCO is a triplet of a linear geometry, with two unpaired electrons occupying two degenerate π orbitals.[6,8,17–20] This motif puts OCCO into the same diradical class as O_2, but there are significant differences. Promoted by the bending motion which distorts OCCO from its linear equilibrium, the triplet undergoes an intersystem crossing (ISC) to a nearby singlet, which promptly dissociates to two CO fragments.[7,17,21] Although the CO + CO asymptote lies >2 eV lower than the triplet OCCO minimum,[17,18] the enabling ISC takes about half a nanosecond to occur,[7] giving OCCO a spectroscopically long lifetime. In this work, we continue the analysis of the OCCO anion photoelectron spectrum, present its detailed Franck-Condon analysis, which reinforces our initial findings and conclusions,[6] and put it in the context with the spectroscopy of a related radical species, HOCCO.

The photoelectron spectrum of $HOCCO^-$ emerged quite unexpectedly from the experiment intended to target $OHCCO^-$ (glyoxalide). The ions were generated using a variation of the same O^- chemistry that leads to the formation of $OCCO^-$,[22,23] only instead of H_2^+ abstraction it involves a single deprotonation of the glyoxal precursor. For clarity and for historical reasons, we note that *glyoxalide* ($OHCCO^-$) should not be confused with *glyoxylide*. The former is the deprotonated-glyoxal ion (glyoxal-ide), while glyoxylide is the name given to an infamous homeopathic wonder-drug from the 1940s, long ago classified as fraud by the U.S. Food and Drug Administration.[24] Ironically, the active ingredient of glyoxylide was claimed to be "O=C=C=O,"[24] i.e., ethylenedione, a molecule whose transient nature is now well-established.[7] Although both OCCO (the molecule) and glyoxalide (the $OHCCO^-$ ion) are investigated here,

a)Email: sanov@u.arizona.edu

glyoxylide (the drug) has no connection to the present work.

Single deprotonation of glyoxal was expected to yield glyoxalide, but the observed product proved to be a mixture of $OHCCO^-$ and $HOCCO^-$, with glyoxalide being the minor species. The dominant isomer, $HOCCO^-$ (ethynediolide) is the conjugate base of ethynediol (acetylenediol), which is a popular addition to anionic surfactant mixtures.[25] Ethynediol has been detected directly by infrared spectroscopy,[26] and its cation has been observed by mass-spectrometry.[27,28] Similar works exist on the singularly substituted ethynol (hydroxyacetylene),[29,30] but $HOCCO^-$ and the corresponding neutral radical have not been studied previously. In our experiment, $HOCCO^-$ could, in principle, be formed as a product of glyoxalide rearrangement, $OHCCO^- \rightarrow HOCCO^-$, but the analysis shows that this is unlikely to be the case. Instead, we propose an alternative mechanism for $HOCCO^-$ formation in the O^- reaction with glyoxal.

The presence of the two anion isomers, $OHCCO^-$ and $HOCCO^-$, creates an opportunity to study the corresponding radical species, HOCCO and OHCCO, by themselves, in comparison to each other, and in comparison to OCCO. The comparison to OCCO, in particular. allows us to draw conclusions about the relative degrees of the distortion of the ethylenedione framework due to the addition of an extra hydrogen atom bound to a carbon or an oxygen.

The analysis of the experimental results presented in this work relies on the electronic structure calculations for both the anions and the corresponding neutral radicals and diradicals. Such species are often described by dense manifolds of low-lying states with inherently multi-configurational electronic wavefunctions and present considerable challenges for calculations. We address these challenges using the equation-of-motion (EOM) ionization-potential (IP) and spin-flip (SF) methods, in conjunction with the coupled-cluster theory (CCSD).[31–35]

II. EXPERIMENTAL AND THEORETICAL METHODS

The photoelectron imaging spectrometer and the experimental procedures used for this work have been described in detail elsewhere.[6,36] Briefly, commercial glyoxal solution (Acros Organics, Inc., 40 wt. % in water) was dehydrated for ~12 h using a 1:1 volume ratio of 3 Å molecular sieves. The solution was then decanted and transferred to the sample holder of the instrument, where it was heated to ~50 °C to increase the vapor pressure. The vapor was seeded in an N_2O carrier gas at ~25 psi. The resulting mixture was pulsed into the high-vacuum ion-source chamber using a General Valve, Inc., Series 99 supersonic valve, operating at 50 Hz to match the repetition rate of the laser system.

The supersonic expansion was crossed at a right angle with a continuous ~1 keV electron beam to create plasma. Dissociative electron attachment to N_2O produced O^- anions, which further reacted[22,23,37] with glyoxal to produce mass-to-charge (m/z) 56 and 57 anions. Anions were extracted into the time-of-flight mass spectrometer using a repeller plate pulsed from 0 to −950 V and further accelerated to ~3.5 kV total potential.[36] 532 or 355 nm laser pulses from a Spectra Physics, Inc., LAB-130-50 Nd:YAG laser were timed to interact with the desired mass-to-charge anion packets within the velocity-map[38] imaging[39] assembly.[36] Photoelectrons were projected by a series of velocity-mapping electrodes in the direction mutually perpendicular to the ion and laser beams. Photoelectrons were detected by a position-sensitive dual-MCP detector in a Chevron configuration, coupled to a P43 phosphor screen. The photoelectron images were recorded using a thermoelectrically cooled CCD (Photometrics, Inc., CoolSnap Myo). Raw images were collected typically for $\sim 1 \times 10^6$ experimental cycles and reconstructed using the inverse Abel transformation[40] implemented in BASEX.[41] Radial distributions were calibrated using the well-known electron affinity (EA) of atomic oxygen.[42,43]

Geometry optimizations and harmonic frequency calculations for the OCCO, HOCCO, and OHCCO neutral and anion species were carried out at the CCSD/aug-cc-pVTZ level using the Gaussian 09 software package.[44] Normal mode analysis was performed on the fully optimized structures and further used for Franck-Condon simulations. These simulations were carried out using the PESCAL 2010 software, with the normal modes treated as uncoupled harmonic oscillators with full Duschinsky rotation using the Chen method.[45,46] EOM-XX-CCSD calculations, where XX = SF or IP, were performed using the Q-Chem 4.0 software package,[47] using the geometries optimized at the CCSD/aug-cc-pVTZ level as described above.

III. EXPERIMENTAL RESULTS

We begin with comparative spectroscopy of HOCCO and OCCO. Figure 1 presents the 532 and 355 nm photoelectron spectra of the $m/z = 57$ (predominantly $HOCCO^-$, as discussed below) and $m/z = 56$ ($OCCO^-$) anions. The spectra are plotted versus electron binding energy (eBE), defined as eBE = $h\nu$ − eKE, where eKE is the electron kinetic energy. The $HOCCO^-$ spectra are new, while the $OCCO^-$ results were reported recently in our initial report on the discovery of the ethylenedione molecule.[6] Despite some revealing similarities between the $m/z = 57$ and $m/z = 56$ spectra, their comparison confirms that they are indeed unique and correspond to distinct species. In support of this conclusion, there was no overlap between the $m/z = 57$ and $m/z = 56$ peaks in the parent-ion mass-spectrum. The intensities of the respective mass-peaks were in an approximately 1:2 ratio; therefore, there can be only a minor contribution of ^{13}C substituted $OCCO^-$ at $m/z = 57$ (2% of $OCCO^-$ intensity).

The bulk of $m/z = 57$ anions may include two distinct isomers: $OHCCO^-$ (deprotonated glyoxal) and the rearrangement product $HOCCO^-$ (conjugated base). The analysis in Section IV suggests that the observed spectra correspond predominantly to $HOCCO^-$, with only a minor contribution attributed to $OHCCO^-$. The corresponding band assignments are presented in Figure 2. For clarity, the $HOCCO^-$ spectra in Figure 2 are reproduced from Figure 1 without overlay with the $OCCO^-$ results. Also included in Figure 2 are the raw and Abel-inverted photoelectron images.

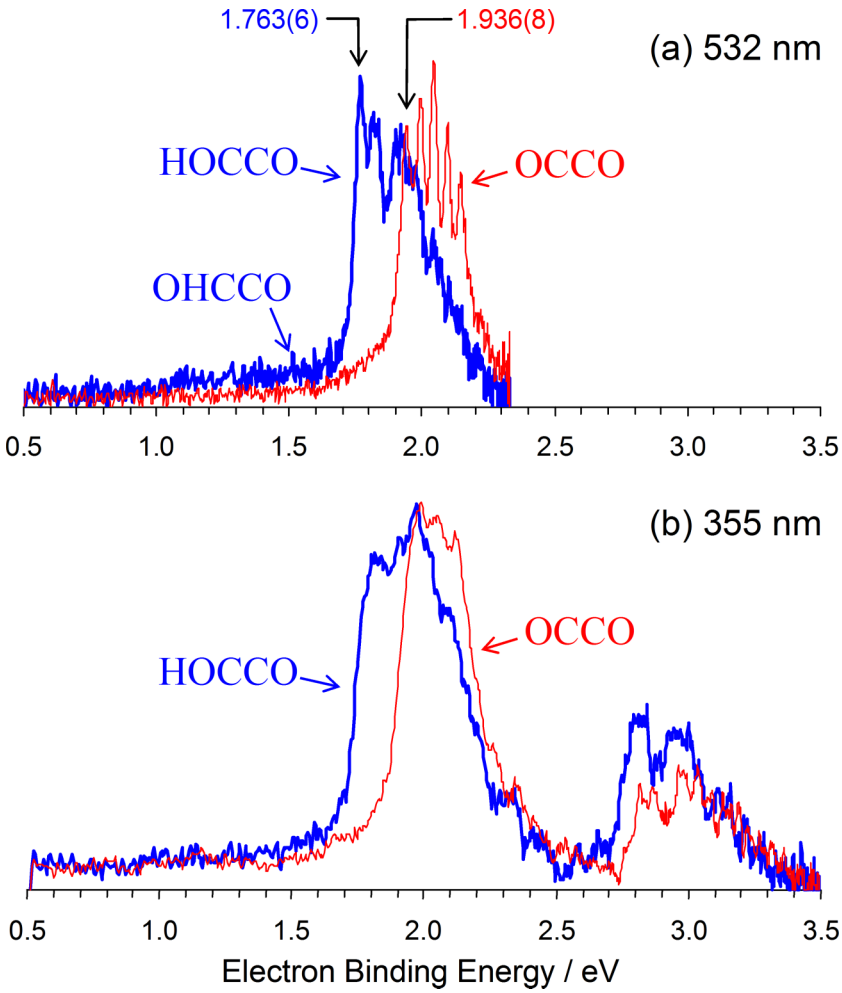

FIG. 1. Comparison of the 532 nm (a) and 355 nm (b) photoelectron spectra of $OCCO^-$ (in red) and $HOCCO^-/OHCCO^-$ (in blue). Electron affinities for the indicated bands are given in eV.

The 532 nm $HOCCO^-$ spectrum in Figure 2(a) includes two main features: a broad low-intensity band A, with an apparent onset at eBE ≈ 1 eV, and a significantly more intense band B that rises sharply at eBE ≈ 1.7 eV and includes a hint of a vibrational progression. In Section IV B, we show that band A corresponds to the $OHCCO^-$ isomer, while the more intense band B, as well as C [in Figure 2(b)], to $HOCCO^-$. The first peak of band B (labeled 1) is observed at 1.763(6) eV, as indicated in Figure 1(a), compared to the first peak in the triplet OCCO progression, which is observed at 1.936(8) eV. Partially resolved peaks 1, 2, and 3 [Figure 2(a)] belong to the dominant vibrational progression with a fundamental frequency of 430(10) cm^{-1}. Additional lower-frequency modes are excited too, contributing to the satellite peaks to the right of peaks 1, 2, and 3.

Band B's vibrational structure is also discernable in the 355 nm spectrum [Figure 2(b)], although the decreased absolute resolution (due to higher eKEs) prevents detailed analysis of the corresponding features. Fitting the envelope of band B in Figure 2(b) with a single Gaussian function places the vertical detachment energy (VDE) at 1.93(4) eV. Band A is weak, but also discernable at 355 nm. An additional spectral band C appears at a higher energy, with a maximum at approximately 2.8 eV. It bears a partially resolved vibrational progression with a ~1300 cm^{-1} spacing between the first two prominent peaks.

In the photoelectron images included in Figure 2, all three bands A, B, and C exhibit strong negative anisotropies with respect to laser polarization direction.

IV. DISCUSSION

A. The anion photoelectron spectrum of OCCO

As proposed previously,[6] the vibrational progression in the 532 nm photoelectron spectrum of $OCCO^-$ [Figure 1(a)] corresponds to the quasi-bound triplet state (T_0) of neutral ethylenedione, while the broad pedestal with the tail extending below the triplet's EA is assigned to a singlet state (S_1), which promptly dissociates into two CO fragments.[7,17,21]

The adiabatic EA of triplet ($^3\Sigma_g^-$) ethylenedione was determined in our original report based on the position of the first peak of the vibrational progression: EA = 1.936(8) eV.[6] This value is indicated in Figure 1(a). The observed spectral progression is consistent with the predicted geometry difference between the $OCCO^-$ anion and triplet OCCO. The equilibrium geometries of these species, optimized at the CCSD level of theory with the aug-cc-pVTZ basis set, are shown in Figure 3. The S_1 pedestal underlying the triplet progression and extending below the triplet EA value reflects the dissociative nature of the singlet, which correlates to the $CO(^1\Sigma^+) + CO(^1\Sigma^+)$ limit some 2.55 eV below the triplet

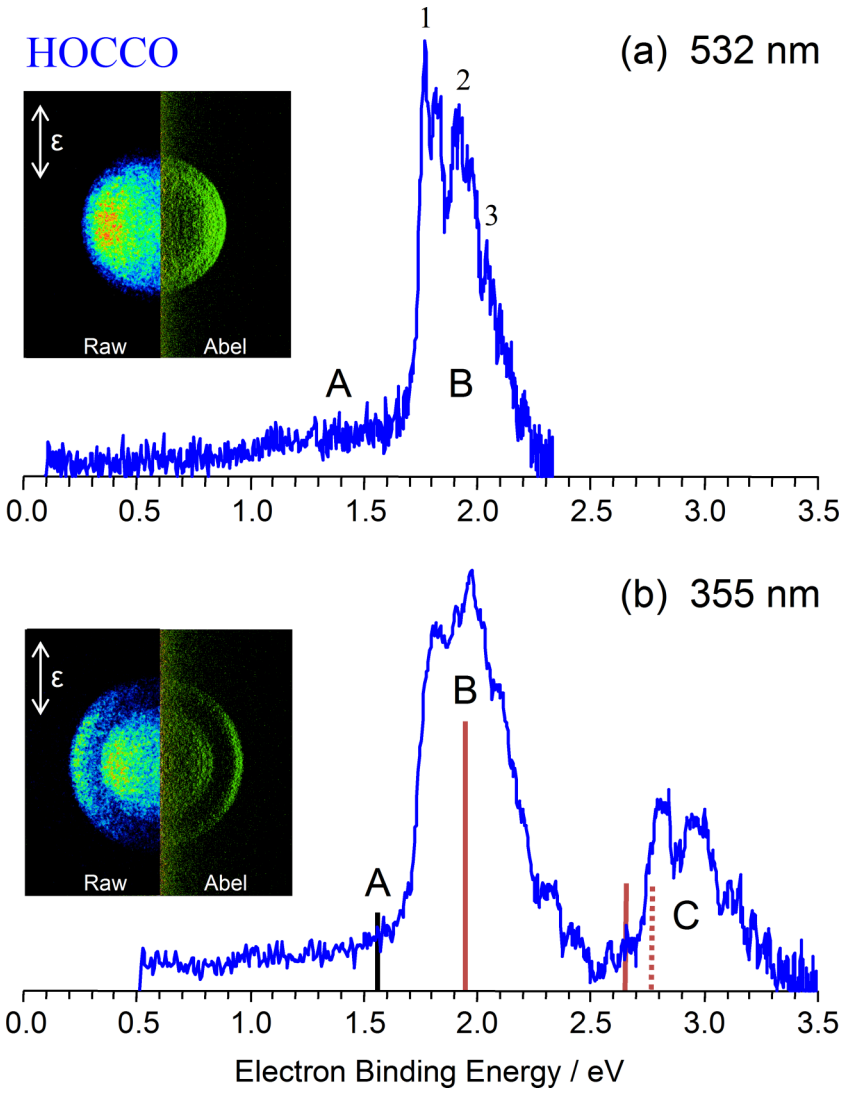

FIG. 2. The 532 nm (a) and 355 nm (b) anion photoelectron spectra of the HOCCO/OHCCO radical system, along with the corresponding photoelectron images. Spectral band A corresponds to detachment from $OHCCO^-$, while Band B and C are attributed to $HOCCO^-$ (see Section IV B for details). The solid vertical bars indicate the computed EOM-IP-CCSD/aug-cc-pVTZ vertical detachment energies for the $OHCCO^-$ (A) and $HOCCO^-$ ((B) and (C)) species. The dashed bar (C) indicates the combined EOM-IP/SF-CCSD result for $HOCCO^-$. The photoelectron images are shown on a split scale, representing the raw (left halves) and Abel-inverted (right halves) data, using different arbitrary color schemes chosen for presentation clarity. The direction of laser polarization is indicated by the double-sided arrows.

equilibrium.[16] While the dissociation limit has no measurable Franck-Condon overlap with the $OCCO^-$ anion, the extended spectral tail reflects the repulsive nature of the singlet surface.

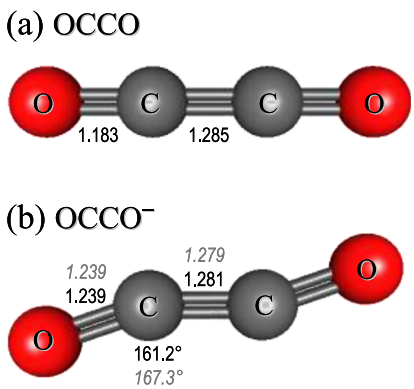

FIG. 3. Optimized geometries of OCCO neutral (a) and anion (b). Bond lengths (in Angstroms) and bond angles from CCSD/aug-cc-pVTZ calculations are shown in plain font; italicized values are the adjusted anion parameters from fitting the Franck-Condon simulation to the experimental data.

We now support the above assignments with a detailed quantitative analysis of the OCCO anion photoelectron spectrum. The final simulation result is shown in Figure 4(a), where the simulated spectrum (black) is overlaid for comparison with the 532 nm experimental spectrum reproduced from Figure 1(a). The simulated spectrum is a sum of the triplet (T_0) vibrational progression and the lowest dissociative-singlet (S_1) band. The separated T_0 and S_1 components of the simulation are shown in Figure 4(b).

The T_0 band was modeled as follows. The fundamental harmonic vibrational frequencies of the triplet neutral and the anion were calculated at the CCSD level with the aug-cc-pVTZ basis set. To avoid issues with the differing numbers of vibrational degrees of freedom of the linear neutral and *trans*-bent anion, the neutral structure was perturbed from its equilibrium geometry by setting ∠CCO to 179.6°, thus reducing its symmetry from $D_{\infty h}$ to C_{2h}. The Franck-Condon (FC) factors were calculated using the PESCAL program.[45,46] The origin (0–0) transition was adjusted to coincide with the maximum of the first vibrational peak of the observed triplet band and the starting *ab initio* anion geometry was adjusted to match the experimental spectrum. This adjustment occurs by fitting the displacements along the neutral normal modes to

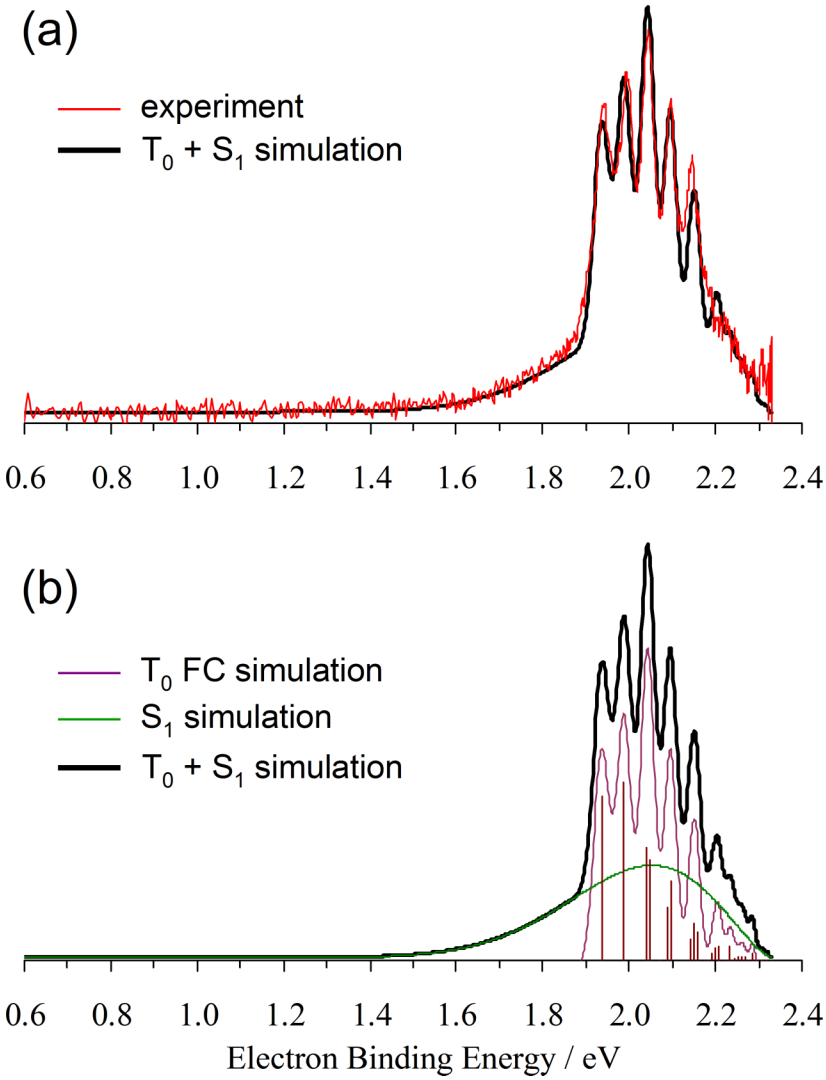

FIG. 4. (a) Simulated 532 nm photoelectron spectrum of $OCCO^-$ (black), overlaid with the experimental spectrum (red) reproduced from Figure 1(a). (b) The overall simulated spectrum from (a) decomposed into the T_0 (purple) and S_1 (green) components, with correspond to the triplet and singlet states of neutral OCCO, respectively. The vertical bars correspond to the simulated Franck-Condon transitions belonging to the T_0 band, while the smooth purple spectrum represents the convolution of the stick spectrum with an instrumental resolution function. The S_1 band is represented by a Wigner-scaled Gaussian function. See text for details.

match the FC simulation to the experimental spectral profile. The calculated FC intensities were multiplied by an $eKE^{3/2}$ pre-factor, accounting for the expected Wigner-like[48] scaling of the electronic part of the photodetachment cross section.[49] The scaling factor used is the same as that adopted in the modeling of the S_1 band in our original report.[6] The final scaled FC stick spectrum is included in Figure 4(b) and the adjusted geometric parameters of the anion are included in Figure 3(b) in *italics* for direct comparison to the *ab initio* predictions.

The FC stick spectrum was convoluted with an instrumental resolution function. The convolution was carried out in the velocity (speed) domain, which corresponds directly to the radial distributions derived from the Abel-inverted photoelectron images. The resolution function was taken to be a Gaussian of a FWHM = 2×10^4 m/s, as determined from O^- photodetachment under similar experimental conditions. The convoluted spectrum was then transformed into the eBE domain using the appropriate Jacobian. The result is shown in Figure 4(b) in purple.

The modeling of the singlet band was described previously.[6] To reiterate, the broad spectral pedestal associated with the dissociative S_1 state of OCCO was described using a Gaussian FC envelope defined in the energy domain, scaled with an $eKE^{3/2}$ Wigner[48] pre-factor.[6,49] This envelope is shown in Figure 4(b) in green. The unscaled Gaussian was centered at the calculated VDE of 2.433 eV,[6] while the width was adjusted to match the simulated band to the experimental spectrum. The green (S_1) and purple (T_0) curves in Figure 4(b) were combined to yield the overall simulated spectrum shown as a bold black curve in both Figures 4(a) and 4(b). Figure 4(a) compares the simulation to the experimental photoelectron spectrum of $OCCO^-$ and we conclude that the analysis presented here is completely consistent with the experimental results.

B. HOCCO/OHCCO radicals via the $HOCCO^-/OHCCO^-$ system photodetachment

The m/z = 57 anion, whose spectra are shown in blue in Figures 1 and 2, can be ascribed as two distinct isomers: (i) the glyoxalide anion $OHCCO^-$, obtained by single deprotonation of the glyoxal molecule; and (ii) $HOCCO^-$, the conjugate base of 1,2-ethynediol (acetylenediol), HO–C≡C–OH. A possible mechanism for the formation of $HOCCO^-$ from glyoxal in our experiment is proposed in Section IV C.

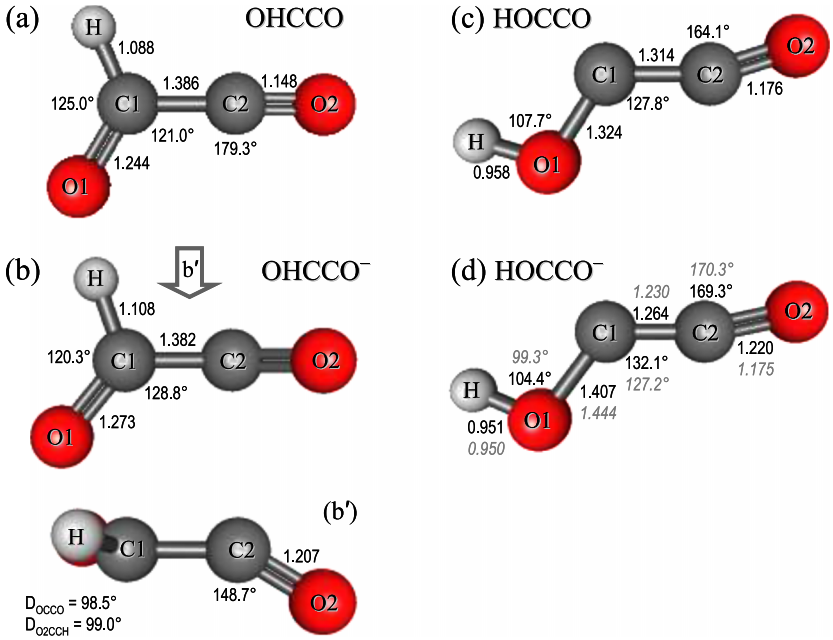

FIG. 5. Optimized structures of (a) OHCCO, ((b) and (b′)) $OHCCO^-$, (c) HOCCO, and (d) $HOCCO^-$. Bond lengths (in Angstroms) and bond angles from CCSD/aug-cc-pVTZ calculations are shown in plain font; italicized values are the adjusted parameters for $HOCCO^-$ from fitting the Franck-Condon simulation to the experimental data.

The structures of $OHCCO^-$, $HOCCO^-$, and the corresponding neutral radicals OHCCO and HOCCO were optimized at the CCSD level of theory with the aug-cc-pVTZ basis set. The resulting equilibrium geometries are shown in Figure 5. For OHCCO, the neutral structure (a) is planar, while the anion is not. The non-planar $OHCCO^-$ is shown in two different projections, (b) and (b′). The OHCCO and $OHCCO^-$ geometries also differ considerably along the O1-C1-C2 dangling angle: 179.3° in the neutral (a) vs. 148.7° in the anion (b′). The HOCCO (c) and $HOCCO^-$ (d) geometries, on the other hand, are significantly more similar to one another.

Single-point EOM-IP-CCSD/aug-cc-pVTZ calculations were performed on the optimized $OHCCO^-$ and $HOCCO^-$ geometries shown in Figures 5(b) and 5(d). The respective closed-shell singlet anion configurations were used as wavefunction references. EOM-IP is non-conserving method with respect to the number of electrons, as it removes one electron from the reference to form target states. When applied to anions, it nominally corresponds to vertical detachment transitions, provided that the target state can be described from the anion reference used. We previously used the same methodology for the ethylenedione system.[6]

According to the EOM-IP calculations for $OHCCO^-$ photodetachment, the two lowest transitions (which nominally correspond to the removal of an electron from the respective HOMO and HOMO–1 of the anion) are found at 1.559 eV and 3.855 eV. The next transition (corresponding to HOMO–2 detachment) is much higher in energy, at 6.360 eV. The energy of the lowest predicted transition (VDE = 1.559 eV) is indicated with the vertical bar next to label A in Figure 2(b). It does not match particularly well the position of band B in the experimental spectra in both Figures 2(a) and 2(b). It is, however, consistent with the weak band A, appearing as the lower-eBE tails in both spectra. Moreover, the onset of this tail, appearing just above 1 eV, is consistent with the adiabatic electron affinity (EA) of OHCCO, calculated as EA = 1.034 eV at the CCSD/aug-cc-pVTZ level, while the very gradual nature of the band's onset is consistent with the large geometry change between $OHCCO^-$ and the corresponding neutral equilibrium [Figures 5(a) and 5(b)]. Hence, band A, rather than band B, is the more likely candidate for the lowest photodetachment transition of the glyoxalide anion, leaving band B to be explained by something else. Similarly, none of the glyoxalide → glyoxalyl transitions predicted by the EOM-IP method can explain band C in the 355 nm spectrum in Figure 2(b).

To explain the origin of the dominant spectral bands B and C in Figure 2, we momentarily return to the comparison of the $OCCO^-$ and $HOCCO^-$/$OHCCO^-$ anion photodetachment in Figure 1. The qualitative parallels between the two spectra suggest that perhaps the addition of hydrogen to an *oxygen* in $OCCO^-$ to form $HOCCO^-$, rather than to a carbon to form $OHCCO^-$, could explain the results, since the former would be a weaker perturbation of the $OCCO^-$ framework compared to glyoxalide.

The structural properties of the $HOCCO^-$ anion (the conjugate base of ethynediol) have not been studied at all, although the neutral acid has been identified in the gas phase.[26] Similarly, no information is available thus far about the corresponding neutral radical species, HOCCO. To shed light on these species, we analyzed the HOCCO radical using the same theoretical procedures as described above for OHCCO.

Turning to Figure 5, the relative similarity of the HOCCO (c) and $HOCCO^-$ (d) structures, as opposed to the dissimilar OHCCO (a) and $OHCCO^-$ (b) geometries, is consistent with the narrow and even partially vibrationally resolved structure of Band B in Figure 2. The lowest photodetachment transitions, predicted by the EOM-IP-CCSD/aug-cc-pVTZ calculations at the $HOCCO^-$ geometry using the closed-shell anion reference, are found at VDE = 1.929 eV (HOMO detachment) and 2.656 eV (HOMO−1), corresponding to a ground–excited state splitting of 0.728 eV. The next neutral state is predicted to lie much higher, at a VDE >7 eV.

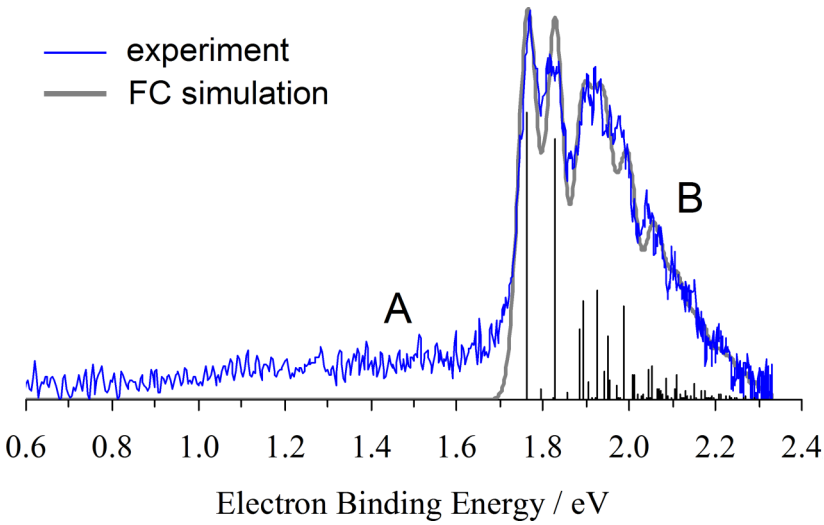

FIG. 6. Simulated Franck-Condon spectrum of $HOCCO^-$ (grey), compared to the 532 nm experimental photoelectron spectrum of the $HOCCO^-$/$OHCCO^-$ system (blue), reproduced from Figure 2(a). The black vertical bars represent the individual Franck-Condon transitions, while the smooth-grey spectrum is obtained by convolution with the instrumental resolution function. See text for details.

The energies of the two lowest predicted transitions are indicated with solid vertical bars B and C in Figure 2(b). The first is in perfect agreement with the experimental VDE of band B, 1.93(4) eV. The second transition, predicted by the EOM-IP calculations to have a VDE of 2.656 eV, coincides with the observed onset of band C in Figure 2(b). Its agreement with the position of band C's maximum (at ~2.8 eV) seems adequate, but leaves more to be desired.

To explore the possibility that the slight discrepancy between the predicted and experimental VDEs to the first excited state of HOCCO is due to non-negligible contributions of electron configurations that are not adequately described by the EOM-IP method with the closed-shell anion reference, we performed additional calculations using the EOM-SF-CCSD methodology. Unlike EOM-IP, spin-flip (SF) is an electron conserving method and hence it cannot describe photodetachment directly. However, it allows access to a variety of doublet configurations starting from the high-spin quartet (triradical) reference,[35] giving a more complete description of the energy splitting between the neutral states.

At the same $HOCCO^-$ anion geometry, the EOM-SF-CCSD/aug-cc-pVTZ calculations predict the lowest excited state of the neutral HOCCO radical (a doublet) to lie at 0.837 eV above the ground state (also a doublet). This state splitting is slightly greater than that predicted by the EOM-IP (0.728 eV), so the SF description of the two states accounts perfectly for the slight EOM-IP discrepancy noted above. By adding the 0.837 eV EOM-SF splitting to the EOM-IP VDE corresponding to the ground HOCCO state (1.929 eV), we predict the VDE to the first excited state to be 2.766 eV, which is in excellent agreement with the experimental maximum of band C (~2.8 eV). The combined EOM-IP/SF result for the first excited state is indicated in Figure 2(b) by the dashed vertical bar.

We also performed a Franck-Condon simulation of the lowest-energy photodetachment transition of $HOCCO^-$ (band B in Figure 2), using the same methodology as described in Section IV A for $OCCO^-$. The harmonic vibrational frequencies of the neutral and anion species of HOCCO were calculated using the CCSD/aug-cc-pVDZ level of theory in Gaussian and were used to generate the $HOCCO^-$ photodetachment spectrum using the PESCAL 2010 program. The output was optimized using the same procedures followed for OCCO, where the 0–0 peak was set to match the first resolved peak of band B in Figure 2(a). The final simulation result is displayed in Figure 6, while the adjusted $HOCCO^-$ structural parameters are included in Figure 5(d) in *italics*, for comparison with the starting CCSD/aug-cc-pVTZ values. Overall, only minor adjustments were needed to be compared to the *ab initio* structure. Similar to Section IV A, the stick spectrum shown in Figure 6 has been scaled with a Wigner pre-factor. It was then convoluted with an experimental broadening function, yielding the smooth spectrum shown in the figure. For comparison, the simulated spectrum is overlaid with the experimental result reproduced from Figure 2(a).

Overall, the quality of the fit in Figure 6 and the agreement of the theoretical VDE predictions with the experiment leave little doubt that band B and band C belong to detachment from $HOCCO^-$. Based on the combination of the experimental and FC simulation results, we assign the EA of the X $^2A''$ state of HOCCO as 1.766(3) eV, with a VDE of 1.93(4) eV. The splitting between the first two partially resolved vibrational peaks of band B is assigned to the in-plane carbon wagging mode of 430(10) cm^{-1}.

C. Formation of ethynediolide, $HOCCO^-$

The unambiguous assignment of bands B and C in the photoelectron spectra of the $m/z = 57$ anion (Figure 2) to the conjugate-base isomer $HOCCO^-$ (ethynediolide) raises the question of this ion's origin in our experiment.

Ethynediol, HOCCOH is not present in the precursor expansion. While it is a metastable tautomer of glyoxal, it is 46.8 kcal mol^{-1} less stable at the CCSD(T)/cc-pVTZ level,[50] so it is unreasonable to expect such a rearrangement in the precursor. The glyoxal tautomerization to ethynediol is predicted to involve the hydroxyketene intermediate,[26] but this species would probably form the glyoxalide anion $OHCCO^-$ more readily than $HOCCO^-$ via the loss of hydrogen from the hydroxyl group rather than the carbon. We conclude that ethynediolide observed in our experiment is not likely to be

formed via a tautomerization reaction involving ethynediol or hydroxyketene.

On the anion surface, $HOCCO^-$ can potentially be formed from glyoxal via two distinct mechanisms. First is a two-step sequential process, whereas the glyoxalide anion is formed first via the expected single deprotonation of glyoxal,

$$OHCCHO + O^- \rightarrow OHCCO^- + OH, \quad (1a)$$

which is followed by the glyoxalide → ethynediolide rearrangement

$$OHCCO^- \rightarrow HOCCO^-. \quad (1b)$$

However, ethynediolide is 12.4 kcal mol^{-1} less stable than glyoxalide (at the CCSD/aug-cc-pVTZ level), making interconversion of nascent $OHCCO^-$ to $HOCCO^-$ unfavorable. Under this mechanism, we would expect a dominant presence of the $OHCCO^-$ anions (responsible for band A in Figures 2 and 6), compared to the less favorable rearrangement product $HOCCO^-$ (responsible for bands B and C).

Instead, we hypothesize that $HOCCO^-$ is formed in an attempt, but failed H_2^+ abstraction from glyoxal, whereas the failure to abstract both hydrogen nuclei creates ethynediolide, rather than glyoxalide, because of a steric rather than energetic propensity,

$$OHCCHO + O^- \rightarrow HO + H\cdots OCCO^- \rightarrow H_2O + OCCO^- \quad (2a)$$

$$\rightarrow HO + HOCCO^-. \quad (2b)$$

Here, $HOCCO^-$ is formed along the same reaction path that leads to $OCCO^-$. The reaction proceeds via an $H\cdots OCCO^-$ complex, from which most trajectories lead to the $OCCO^-$ product ((2a)). Indeed, the $OCCO^-$ ion peak was observed to be significantly more intense than the $m/z = 57$ anion in the parent ion mass-spectrum. Those reaction trajectories that do not possess enough energy to complete path (2a) terminate in the "half-way" $HOCCO^-$ product along path (2b). The planar OCCO skeleton of glyoxal is a better match to that in $HOCCO^-$ than in $OHCCO^-$. $HOCCO^-$ is also planar, while the OCCO group in relaxed glyoxalide has a significant out-of-plane distortion [Figure 5(b)]. Therefore, when the almost abstracted second hydrogen returns to the $OCCO^-$ skeleton along path (2b), it tends to form ethynediolide rather than glyoxalide, because of the comparatively small rearrangement of the heavy atoms required in this case.

By the same reasoning, formation of glyoxalide by single deprotonation of glyoxal is unfavorable due to the large geometry change needed to equilibrate the new structure. However, some $OHCCO^-$ may be formed via this mechanism or a subsequent $HOCCO^- \rightarrow OHCCO^-$ rearrangement to explain the presence of the weak band A in the spectra in Figures 2 and 6.

D. HOCCO versus OCCO

Finally, we comment on the parallels between the properties of $OCCO^-$ and $HOCCO^-$, as well as the corresponding neutral species. The qualitative similarity of the photoelectron spectra in Figure 1 is striking, but not surprising.

The calculated electron affinities of HOCCO and OCCO differ by only 0.17 eV, in agreement with the experimental data in Figure 1. The first excited state of HOCCO [band C in Figure 2(b)] and the S_3 state of OCCO differ in VDE by a similarly small amount [see Figure 1(b)]. In the anion state, both $HOCCO^-$ and $OCCO^-$ have similar *trans*-bent geometries of the OCCO skeleton [Figures 5(d) and 3(b), respectively]. Both species undergo a contraction of the O–C bonds upon electron detachment, with HOCCO also experiencing a significant elongation of the C–C bond relative to the anion, much more pronounced than in OCCO. By far the greatest difference between the OCCO and HOCCO structures is the overall similarity of the HOCCO geometry to its anion. $OCCO^-$ changes from *trans*-bent to linear upon photodetachment to the ground (triplet) state of the neutral diradical, while the HOCCO radical retains the *trans*-bent configuration of its anion.

Considering the calculated energetics and geometries, OCCO is much more similar to HOCCO than to OHCCO. This observation supports our assignment of the $m/z = 57$ ions as predominantly $HOCCO^-$, rather than $OHCCO^-$. Qualitatively, the addition of a hydrogen to an oxygen in OCCO can be thought of as a relatively minor perturbation, compared to H bonding to one of the carbon atoms. As seen in Figure 5, the formation of a C–H bond significantly distorts the heavy-atom skeleton of the molecule, especially in the anion, much more so than the formation of an O–H bond at one of the terminal atoms.

V. SUMMARY AND FUTURE DIRECTIONS

We presented a comparative anion photoelectron imaging study of a family of exotic glyoxal-derived species, including the OCCO diradical and the radical species HOCCO and OHCCO. The main spectral features can be summarized as follows. The 532 nm photoelectron spectrum of $OCCO^-$ [Figure 1(a)] features a vibrational progression assigned to the (quasi-) bound triplet state of OCCO.[6] Detailed analysis of the spectrum, including the Franck-Condon simulation of the triplet-state vibrational progression, confirms the previously determined EA of triplet OCCO, EA = 1.936(8) eV. The broad spectral pedestal underlying the progression is due to the dissociative singlet state of OCCO, while the higher-energy band observed at eBE ~3 eV at 355 nm is assigned to a higher-lying singlet state.[6]

The photoelectron spectra of the $m/z = 57$ anion include contributions of the $OHCCO^-$ (glyoxalide) and $HOCCO^-$ (ethynediolide) isomers, with $HOCCO^-$ being the dominant species. Similar to OCCO, the 532 nm spectrum [Figures 1(a) and 2(a)] also features a partially resolved vibrational progression, which is assigned to the ground state of the HOCCO radical. This assignment came as an initial surprise, because direct deprotonation of the glyoxal precursor was expected to yield the glyoxalide anion, $OHCCO^-$. The adiabatic EA of the HOCCO radical is determined to be

1.763(6) eV, slightly smaller in magnitude than that of triplet OCCO. The spectrum also shows a weak but broad low-eBE tail (band A in Figure 2), which is similar in appearance to the dissociative-state pedestal in the OCCO spectrum. In contrast to OCCO, this tail is attributed to a different isomer of the anion, $OHCCO^-$, rather than to a dissociative neutral state. The higher-energy band observed in the 355 nm $OHCCO^-/HOCCO^-$ spectrum is attributed to an excited state of HOCCO.

Although as explained in Section IV C the dominance of the $HOCCO^-$ bands in the spectra was unexpected, the analysis, supported by FC simulations and electronic-structure calculations, leaves little doubt that $HOCCO^-$ is indeed the major $m/z = 57$ anion product observed in the reaction of glyoxal with O^-. We proposed a mechanism for this reaction, which involves a *failed* abstraction of H_2^+ (en route to the $OCCO^-$ product) that terminates in H^+ (rather than H_2^+) abstraction and favors the formation of $HOCCO^-$ over $OHCCO^-$ due to geometric constraints. Further theoretical study of this reaction, possibly using transition-state theory and semi-classical trajectory calculations, could lead to a more complete understanding of the origins of the $HOCCO^-$ anion, and preliminary discussions of such calculations are currently under way. Moreover, the qualitative mechanism proposed here may prove to be more general, with implications to a broader class of organic reactions. On the experimental side, measurements of anionic fragmentation products, provided such pathways exist, could also help to unambiguously differentiate between the $HOCCO^-$ and $OHCCO^-$ isomers. Isotopically substituted glyoxal, glyoxal-d_2, or the addition of D_2O to the sample mixture may provide some insight into possible formation mechanisms. Inhibition of $HOCCO^-$ formation or a change in relative photoelectron intensity between $HOCCO^-$ and $OHCCO^-$ would be illuminating, and be a good complement to the aforementioned theoretical approach.

The parallels between the anion photoelectron spectra of the HOCCO radical and the OCCO diradical result from the relatively minor perturbation caused by the hydrogen addition to an oxygen in OCCO. Conversely, the addition of a hydrogen to the carbon frame results in a much more severe perturbation and a large geometry change predicted for OHCCO and the corresponding anion. The low-lying states of OHCCO and HOCCO remain largely unexplored, although their reactivity may prove important to atmospheric and combustion chemistry, due to the ubiquitous nature of glyoxal. We reiterate[6] that future experiments targeting the lifetime of OCCO and the energy exchange in its unimolecular decomposition will provide insight into the fundamental properties of this intriguing molecule.[7,8]

ACKNOWLEDGMENTS

We thank Dr. Dmitry Khuseynov for his encouragement to use glyoxal as the precursor in this work. William P. Brezinski and Dr. Richard F. Vreeland are acknowledged for their help with dehydration of the precursor. We are also pleased to acknowledge the generous support of this work by the U.S. National Science Foundation (Grant No. CHE-1266152).

[1]K. M. Ervin and W. C. Lineberger, "Photoelectron spectroscopy of negative ions," in *Advances in Gas Phase Ion Chemistry*, edited by N. G. Adams and L. M. Babcock (JAI Press, Greenwich, 1992), Vol. 1, pp. 121–166.
[2]P. G. Wenthold and W. C. Lineberger, Acc. Chem. Res. **32**, 597 (1999).
[3]D. N. Neumark, Science **272**, 1446 (1996).
[4]D. M. Neumark, Phys. Chem. Chem. Phys. **7**, 433 (2005).
[5]L. M. Culberson, A. A. Wallace, C. C. Blackstone, D. Khuseynov, and A. Sanov, Phys. Chem. Chem. Phys. **16**, 3964 (2014).
[6]A. R. Dixon, T. Xue, and A. Sanov, Angew. Chem., Int. Ed. **54**, 8764–8767 (2015).
[7]D. Schröder, C. Heinemann, H. Schwarz, J. N. Harvey, S. Dua, S. J. Blanksby, and J. H. Bowie, Chem. Eur. J. **4**, 2550 (1998).
[8]E. G. Lewars, "Ethenedione, C_2O_2," in *Modeling Marvels* (Springer, 2008), pp. 131–140.
[9]H. Staudinger and E. Anthes, Ber. Dtsch. Chem. Ges. **46**, 1426 (1913).
[10]J. A. Berson, D. M. Birney, W. P. Dailey, and J. F. Liebman, in *Modern Models of Bonding and Delocalization, Molecular Structures and Energetics*, edited by J. F. Liebman and A. Greenberg (VCH, Weinheim, 1988), Vol. 6, p. 391.
[11]M. B. Rubin, A. Patyk, and W. Sander, Tetrahedron Lett. **29**, 6641 (1988).
[12]D. Sulzle, T. Weiske, and H. Schwarz, Int. J. Mass Spectrom. Ion Processes **125**, 75 (1993).
[13]L. A. Surin, D. N. Fourzikov, F. Lewen, B. S. Dumesh, G. Winnewisser, and A. R. W. McKellar, J. Mol. Spectrosc. **222**, 93 (2003).
[14]H. W. Chen and J. L. Holmes, Int. J. Mass Spectrom. **133**, 111 (1994).
[15]W. E. Thompson and M. E. Jacox, J. Chem. Phys. **95**, 735 (1991).
[16]J. R. Thomas, B. J. DeLeeuw, P. O'Leary, H. F. Schaefer, B. J. Duke, and B. O'Leary, J. Chem. Phys. **102**, 6525 (1995).
[17]D. Talbi and G. S. Chandler, J. Phys. Chem. A **104**, 5872 (2000).
[18]C. Trindle, Int. J. Quantum Chem. **93**, 286 (2003).
[19]G. P. Raine, H. F. Schaefer, and R. C. Haddon, J. Am. Chem. Soc. **105**, 194 (1983).
[20]N. L. Ma and M. W. Wong, Angew. Chem., Int. Ed. **37**, 3402 (1998).
[21]A. A. Korkin, A. Balkova, R. J. Bartlett, R. J. Boyd, and P. V. Schleyer, J. Phys. Chem. **100**, 5702 (1996).
[22]J. Lee and J. J. Grabowski, Chem. Rev. **92**, 1611 (1992).
[23]J. J. Grabowski and S. J. Melly, Int. J. Mass Spectrom. **81**, 147 (1987).
[24]W. W. Goodrich, Interview for FDA Oral History Program, Part 2, 15 October 1986, U.S. Department of Health and Human Services, Food and Drug Administration History Office, United States Food and Drug Administration, Rockville, Maryland. Available at http://www.fda.gov/downloads/aboutfda/whatwedo/history/oralhistories/selectedoralhistorytranscripts/ucm372999.pdf.
[25]M. K. Hazra, J. S. Francisco, and A. Sinha, J. Phys. Chem. A **118**, 4095 (2014).
[26]G. Maier and C. Rohr, Liebigs Ann. **1996**, 307.
[27]S. Skujins, J. Delderfield, and G. A. Webb, Tetrahedron **24**, 4805 (1968).
[28]J. K. Terlouw, P. C. Burgers, B. L. M. v. Baar, T. Weiske, and H. Schwarz, Chimia **40**, 357 (1986), ISSN: 0009-4293.
[29]B. Vanbaar, T. Weiske, J. K. Terlouw, and H. Schwarz, Angew. Chem., Int. Ed. **25**, 282 (1986).
[30]R. Hochstrasser and J. Wirz, Angew. Chem., Int. Ed. **28**, 181 (1989).
[31]A. I. Krylov, Chem. Phys. Lett. **350**, 522 (2001).
[32]A. I. Krylov, Annu. Rev. Phys. Chem. **59**, 433 (2008).
[33]P. G. Szalay, J. Vazquez, C. Simmons, and J. F. Stanton, J. Chem. Phys. **121**, 7624 (2004).
[34]L. V. Slipchenko and A. I. Krylov, J. Chem. Phys. **117**, 4694 (2002).
[35]A. I. Krylov, Acc. Chem. Res. **39**, 83 (2006).
[36]L. Velarde, T. Habteyes, and A. Sanov, J. Chem. Phys. **125**, 114303 (2006).
[37]J. H. J. Dawson and K. R. Jennings, J. Chem. Soc., Faraday Trans. 2 **72**, 700 (1976).
[38]A. T. J. B. Eppink and D. H. Parker, Rev. Sci. Instrum. **68**, 3477 (1997).
[39]D. W. Chandler and P. L. Houston, J. Chem. Phys. **87**, 1445 (1987).
[40]A. J. R. Heck and D. W. Chandler, Annu. Rev. Phys. Chem. **46**, 335 (1995).
[41]V. Dribinski, A. Ossadtchi, V. A. Mandelshtam, and H. Reisler, Rev. Sci. Instrum. **73**, 2634 (2002).

[42]D. M. Neumark, K. R. Lykke, T. Andersen, and W. C. Lineberger, Phys. Rev. A **32**, 1890 (1985).
[43]S. J. Cavanagh, S. T. Gibson, M. N. Gale, C. J. Dedman, E. H. Roberts, and B. R. Lewis, Phys. Rev. A **76**, 052708 (2007).
[44]M. J. Frisch *et al.*, GAUSSIAN 09, Gaussian, Inc., Wallingford, CT, 2009.
[45]K. M. Ervin, T. M. Ramond, G. E. Davico, R. L. Schwartz, S. M. Casey, and W. C. Lineberger, J. Phys. Chem. A **105**, 10822 (2001).
[46]P. Chen, in *Unimolecular and Bimolecular Reactions Dynamics*, edited by C.-Y. Ng, T. Baer, and I. Powis (John Wiley & Sons, Chichester, 1994), p. 371.
[47]Y. Shao *et al.*, Phys. Chem. Chem. Phys. **8**, 3172 (2006).
[48]E. P. Wigner, Phys. Rev. **73**, 1002 (1948).
[49]D. Khuseynov, A. R. Dixon, D. J. Goebbert, and A. Sanov, J. Phys. Chem. A **117**, 10681 (2013).
[50]D. Vijay and G. N. Sastry, J. Mol. Struct. **714**, 199 (2005).